Selective Substitution of Cr in CaFe$_4$As$_3$ and Its Effect on the Spin Density Wave

Iliya Todorov,[†] Duck Young Chung,[†] Helmut Claus,[†] Kenneth E. Gray,[†]
Qing'an Li,[†] John Schleuter,[†] Thomas Bakas,[§] Alexios P. Douvalis,[§]
Matthias Gutmann,[⊥] and Mercouri G. Kanatzidis*[,†,‡]

[†]*Materials Science Division, Argonne National Laboratory, Argonne, Illinois 60439,* [‡]*Department of
Chemistry, Northwestern University, Evanston, Illinois 60208,* [§]*Department of Physics,
University of Ioannina, 45110 Ioannina, Greece, and* [⊥]*Rutherford Appleton Laboratory,
Harwell Science and Innovation Campus, ISIS Facility, Oxfordshire, United Kingdom*

Received May 5, 2010. Revised Manuscript Received July 15, 2010

Single crystals of CaCr$_{0.84}$Fe$_{3.16}$As$_3$, a Cr substituted analog of CaFe$_4$As$_3$, were grown from Sn flux and characterized with single crystal neutron diffraction. CaCr$_{0.84}$Fe$_{3.16}$As$_3$ crystallizes in the orthorhombic space group *Pnma* with a three-dimensional framework, where Fe, Cr, and As form a covalent channel-like network with Ca^{2+} cations residing in the channels. CaCr$_{0.84}$Fe$_{3.16}$As$_3$ has a unit cell of $a = 12.057(4)$ Å, $b = 3.7374(13)$ Å, and $c = 11.694(3)$ Å, as determined by room temperature single crystal neutron diffraction ($R_1 = 0.0747$, w$R_2 = 0.1825$). Structural data was also collected at 10 K. The single crystal neutron data showed that Cr selectively occupies a particular metal site, Fe(4). The antiferromagnetic transition associated with spin density wave (SDW) in the parent compound is preserved and shifts from 96 to 103 K with the selective Cr doping. Mössbauer, magnetic, and electrical resistivity measurements are reported.

Introduction

The discovery of unconventional superconductivity in SmFeAsO$_{1-x}$F$_x$ spiked extensive interest in layered iron arsenide materials.[1] This superconducting class includes REOFeAs (RE = La, Ce, Pr, Nd, Sm)[2−5] with ZrCuSiAs structure type, AFeAs (A = Li, Na)[6−9] with PbFCl structure type, and (A/AE)Fe$_2$As$_2$, (A = K, Rb, Cs; AE = Sr, Ba)[10−13] with ThCr$_2$Si$_2$ structure type. In these materials, the origin of superconductivity is still unclear but the competition between magnetism and superconductivity or superconductivity mediated by antiferromagnetic (AFM) fluctuations are of intense interest. The former hypothesis was investigated by muon spin rotation (μSR) measurement across the phase boundaries of LaFeAsO$_{1-x}$F$_x$ and CaFe$_{1-x}$Co$_x$AsF where a macroscopic phase separation into superconducting and magnetic phases was found.[14] Superconductivity in these systems occurs by doping or applying high pressure.[15] For example, electron doping in LaFeAsO$_{1-x}$F$_x$ suppresses the structural and magnetic transition associated with a spin-density wave (SDW) in favor of superconductivity already at $x = 0.03$.[16] Fe hole doping in Ba$_{1-x}$K$_x$Fe$_2$As$_2$, the SDW is also suppressed but at a much higher K doping state ($x \sim 0.2−0.3$),[10] which corresponds to the doping of the FeAs layers with 0.15 holes per Fe ion. In addition, the superconductivity in CaFe$_2$As$_2$ (Tc $\sim$ 10 K at 0.69 GPa) is a result of high pressure after the structure undergoes a volume collapse with drastic reduction of its c axis parameter by 9.5%.[17]

(1) Kamihara, Y.; Hiramatsu, H.; Hirano, M.; Kawamura, R.; Yanagi, H.; Kamiya, T.; Hosono, H. *J. Am. Chem. Soc.* **2006,** *128,* 10012.
(2) Kamihara, Y.; Watanabe, T.; Hirano, M.; Hosono, H. *J. Am. Chem. Soc.* **2008,** *130,* 3296.
(3) Takahashi, H.; Igawa, K.; Arii, K.; Kamihara, Y.; Hirano, M.; Hosono, H. *Nature* **2008,** *453,* 376.
(4) Ren, Z.-A.; Che, G.-C.; Dong, X.-L.; Yang, J.; Lu, W.; Yi, W.; Shen, X.-L.; Li, Z.-C.; Sun, L.-L.; Zhou, F.; Zhao, X.-Z. *Europhys. Lett.* **2008,** *83,* 17002.
(5) Nekrasov, I. A.; Pchelkina, Z. V.; Sadovskii, M. V. *JETP Lett.* **2008,** *88*(8), 543.
(6) Chu, C. W.; Chen, F.; Gooch, M.; Guloy, A. M.; Lorenz, B.; Lv, B.; Sasmal, K.; Tang, Z. J.; Tapp, J. H.; Xue, Y. Y. *Phys. C: Supercond.* **2009,** *469,* 326.
(7) Gooch, M.; Lv, B.; Tapp, J. H.; Tang, Z.; Lorenz, B.; Guloy, A. M.; Chu, C. W. *EPL* **2009,** *85,* 27005.
(8) Parker, D. R.; Pitcher, M. J.; Baker, P. J.; Franke, I.; Lancaster, T.; Blundell, S. J.; Clarke, S. J. *Chem. Commun.* **2009,** *16,* 2189.
(9) Kurmaev, E. Z.; McLeod, J.; Skorikov, N. A.; Finkelstein, L. D.; Moewes, A.; Korotin, M. A.; Izyumov, Y. A.; Clarke, S. J., *arXiv:0903.4901v1.*
(10) Rotter, M.; Tegel, M.; Johrendt, D. *Phys. Rev. Lett.* **2008,** *101,* 107006.
(11) Christianson, A. D.; Goremychkin, E. A.; Osborn, R.; Rosenkranz, S.; Lumsden, M. D.; Malliakas, C. D.; Todorov, I.; Claus, H.; Chung, D. Y.; Kanatzidis, M. G.; Bewley, R. I.; Guidi, T. *Nature* **2008,** *456,* 930.
(12) Sasmal, K.; Bing, L.; Lorenz, B.; Guloy, A. M.; Chen, F.; Xue, Y.-Y.; Chu, C.-W. *Phys. Rev. Lett.* **2008,** *101,* 107007.
(13) Chen, G. F.; Li, Z.; Li, G.; Hu, W. Z.; Dong, J.; Zhang, X. D.; Zheng, P.; Wang, N. L.; Luo, J. L. *Chin. Phys. Lett.* **2008,** *25,* 3403.
(14) Takeshita, S.; Kadono, R. *New J. Phys.* **2009,** 11 035006.
(15) Kreyssig, A.; Green, M. A.; Lee, H.; Samolyuk, G. D.; Zajdel, P.; Lynn, J. W.; Bud'Ko, S. L.; Torikachvili, M. S.; Ni, N.; Nandi, S.; Leão, J. B.; Poulton, S. J.; Argyriou, D. N.; Harmon, B. N.; McQueeney, R. J.; Canfield, P. C.; Goldman, A. I. *Phys. Rev. B* **2008,** *78,* 184517.
(16) Dong, J.; Zhang, H. J.; Xu, G.; Li, Z.; Li, G.; Hu, W. Z.; Wu, D.; Chen, G. F.; Dai, X.; Luo, J. L.; Fang, Z.; Wang, N. L. *Europhys. Lett.* **2008,** *83,* 27006.
(17) Chu, C. W.; Lorenz, B. *Phys. C: Supercond.* **2009,** *469,* 385.

Article

Chem. Mater., Vol. 22, No. 17, 2010 4997

Recently, we and others described the new compound, $CaFe_4As_3$, with a complex anisotropic magnetic structure.[18,19] The compound has a network of Fe/As ribbons excised out of the Fe_2As_2 layers in the $ThCr_2Si_2$ structure type superconductors. Similarly to the superconducting phases, $CaFe_4As_3$ shows an AFM-like transition associated with spin density wave (SDW) which occurs around 96 K. The magnetic structure of this compound has been studied by neutron powder diffraction. Long-range magnetic order was detected below 85 K, with an incommensurate modulation described by the propagation vector $k = (0, \delta, 0)$, $\delta \sim 0.39$. Below ~ 25 K, the measurements detect a first-order phase transition where δ locks into the commensurate value $3/8$.[20] In addition, the SDW transition at 96 K is close to the SDW transition temperature observed in $BaFe_2As_2$.[21] Inspired by this, we attempted to modify $CaFe_4As_3$ through atomic substitution in order to suppress or perturb the SDW. We found that $CaFe_4As_3$ is not readily amenable to chemical substitution on any of its atomic sites (i.e., Ca, Fe, and As). After extensive experiments, we were successful only with Cr which can partially substitute in one of the Fe sites in the structure to produce the new compound $CaCr_{0.84}Fe_{3.16}As_3$.

$CaCr_{0.84}Fe_{3.16}As_3$ is isostructural to $CaFe_4As_3$, as determined with room-temperature single-crystal neutron diffraction analysis which is key to determining the location of Cr. It is noteworthy that Cr is not randomly distributed at all crystallographic Fe positions but is exclusively situated at a particular metal site, Fe(4), associated with the Fe^{1+} centers in the compound. The selective Cr-doping may occur on the Fe(4) site because Cr and the Fe^{1+} centers have similar atomic radii; the Fe−As bonds at the Fe(4) site are longer, and the square pyramidal coordination is compatible with the Cr center as shown from calculations of ligand field stabilization energies.[22] This selectivity results in significant changes in the properties of $CaFe_4As_3$ including higher resistivity for $CaCr_{0.84}Fe_{3.16}As_3$ and the disappearance of the 23 K ferromagnetic transition observed in $CaFe_4As_3$.[18,19] It is interesting that the antiferromagnetic transition associated with a SDW at 96 K is preserved and shifts higher at 103 K. The results of extensive investigations aimed at chemical substitution of $CaFe_4As_3$ are described as well as detailed physical characterization including anisotropic electrical resistivity, magnetic susceptibility measurements, and Mössbauer spectroscopy.

Experimental Section

Synthesis. Elements used for the preparation of $CaCr_{0.84}Fe_{3.16}As_3$ were Ca (Alfa Aesar, granules, 99.5%), Cr (Cerac,

powder, 99.9%), Fe (Cerac, powder, 99.9%), As (Alfa Aesar, powder, 99.99%), and Sn (Cerac, shot, 99.9%). All preparations were done in a nitrogen-filled glovebox with moisture and oxygen levels less than 1 ppm.

Synthesis of $CaCr_{0.84}Fe_{3.16}As_3$. Ca (0.1221 g, 3 mmol), Cr (0.1559 g, 3 mmol), Fe (0.5026 g, 9 mmol), and As (0.674 g, 9 mmol) were thoroughly mixed and loaded in an alumina crucible. After 14 g of Sn pieces were added, a plug of alumina wool was then placed on top of the reaction crucible. The alumina crucible was placed in a quartz ampule and subsequently sealed under reduced pressure of 10^{-4} Torr. This assembly was heated to 650 °C for 12 h, held there for a period of 6 h, then heated to 1000 °C for 12 h, and stayed there for 6 h, followed by slow cooling to 600 °C for 48 h. At this temperature, liquid Sn flux was removed by centrifugation. The resulting metallic needle-like crystals obtained at the quantitative yield had a typical dimension of $6.0 \times 1.0 \times 1.0$ mm^3. The purity of the synthesized product was confirmed with Powder X-ray Diffraction (PXRD). No other impurity except a small amount of residual Sn was found in the product.

Structure Determination. A cylindrical single crystal with 1 mm diameter and 6 mm length was mounted on an Al pin using thin strips of adhesive Al tape inside a top-loading closed cycle refrigerator and surrounded by He exchange gas. Data were collected on the neutron time-of-flight Laue single crystal diffractometer SXD installed at the ISIS pulsed neutron source at 300 and 10 K, using 5 and 4 exposures, respectively.[23] The complete data collection parameters, details of structure solution, and refinement results are given in Table 1. For the data collected at 300 K, final atomic positions, displacements parameters, and anisotropic displacement parameters are given in Tables S1 and S2 in the Supporting Information. Selected bond distances and angles are listed in Table S3, Supporting Information.

Electrical Resistivity Measurements. For electrical contacts, Au was sputtered onto the long axis of the crystal (*b* axis) in a pattern of stripes perpendicular to the long dimension of the crystal. Four stripes were placed symmetrically on both the top and bottom surfaces. In the standard six-terminal configuration, the outer stripes on the top supply the current, *I*. Then, the inner stripes on that surface define, V_{top}, and the bottom surface, V_{bot}. Crystals were measured in standard ^{4}He flow cryostat. Heating was avoided by reducing the current, and hysteresis caused by slight thermometer-sample temperature differences was avoided by sweeping the temperature slowly, especially near the transitions. We used six terminals to determine each principal component of resistivity, i.e., parallel to the *b* axis, ρ_b, and perpendicular (*ac* plane), ρ_{ac}.

Magnetic Measurements. Anisotropic magnetization measurements of $CaCr_{0.84}Fe_{3.16}As_3$ single crystals were performed using a Quantum Design MPMS SQUID magnetometer. Aligned single crystals were mounted on a Kapton tape and supported on a plastic straw. Temperature dependent data were collected for both zero field cooled (ZFC) and field cooled modes (FC) between 5 and 300 K, with an applied field of 2000 Oe parallel (χ_b) and perpendicular (χ_{ac}) to the crystal *b* axis. The data were corrected for the holder and for ion-core diamagnetism. Above 103 K, the compound showed Curie−Weiss behavior and the data were fitted with $\chi_m = C/(T - \Theta)$ with accuracies of the fits better than 99%. The following parameters were derived from these fits: $\mu_b = 5.87$ and $\mu_{ac} = 5.44$ Bohr magneton (B.M.).

(18) Todorov, I.; Chung, D. Y.; Malliakas, C. D.; Li, Q.; Bakas, T.; Douvalis, A.; Trimarchi, G.; Gray, K. E.; Mitchell, J. F.; Freeman, A. J.; Kanatzidis, M. G. *J. Am. Chem. Soc.* **2009**, *131*, 5405.

(19) Zhao, L. L.; Tanghong, Y.; Fettinger, J. C.; Kauzlarich, S. M.; Morosan, E. *Phys. Rev. B* **2009**, *80*, 020404.

(20) Manuel, P.; Chapon, L. C.; Todorov, I. S.; Chung, D. Y.; Castellan, J.-P.; Rosenkranz, S.; Osborn, R.; Toledano, P.; Kanatzidis, M. G. *Phys. Rev. B* **2010**, *81*, 184402.

(21) Ni, N.; Bud'ko, S. L.; Kreyssig, A. A.; Nandi, S.; Rustan, G. E.; Goldman, A. I.; Gupta, S.; Corbett, J. D.; Kracher, A.; Canfield, P. C. *Phys. Rev. B* **2008**, *78*, 014507.

(22) Wiberg, E. *Inorganic Chemistry*; Academic Press: San Diego, 2001; pp 1188−1209.

(23) Keen, D. A.; Gutmann, M. J.; Wilson, C. C. *J. Appl. Crystallogr.* **2006**, *39*, 714.

Table 1. Single Crystal Data and Structure Refinements Obtained from Neutron Diffraction for $CaCr_{0.84}Fe_{3.16}As_3$ at Different Temperatures
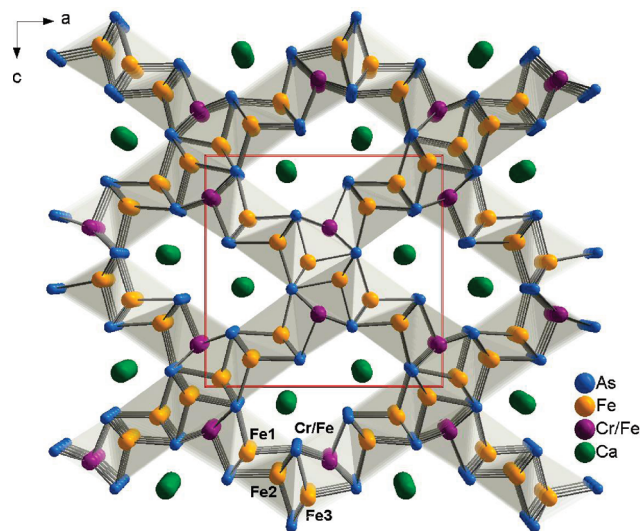
	$CaCr_{0.84}$-$Fe_{3.16}As_3$	$CaCr_{0.84}$-$Fe_{3.16}As_3$
empirical formula		
formula weight	484.97	484.38
temperature, K	10(2)	300(2)
wavelength range, Å	0.35−10.0	0.35−10.0
crystal system	orthorhombic	orthorhombic
space group	*Pnma*	*Pnma*
unit cell dimensions, Å	a = 12.022(4)	a = 12.057(4)
	b = 3.7211(15)	b = 3.7374(13)
	c = 11.652(3)	c = 11.694(3)
volume, Å^3	521.2(3)	526.9(3)
Z	4	4
density (calculated), g/cm^3	6.180	6.106
absorption coefficient, cm^{-1}	$0.438 + 0.104\lambda$	$0.438 + 0.104\lambda$
$F(000)$	229	226
crystal size, mm^3	6.00×1.00	6.00×1.00
	$\times 1.00$	$\times 1.00$
reflections collected	3549	2982
independent reflections [R_{int}]	3549 [0.0000]	2982 [0.0000]
data/restraints/parameters	3549/0/51	2982/0/52
goodness-of-fit on F^2	1.076	1.060
final R_1/wR_2 indices $[F_0^2 > 2\sigma(F_0^2)]^a$, %	8.03/19.74	7.47/18.25
R_1/wR_2 indices ($F_0^2 > 0$), %	8.03/19.74	7.47/18.25

$^a R_1 = \Sigma||F_o| - |F_c||/\Sigma|F_o|$; $wR_2 = [\Sigma w\{|F_o| - |F_c|\}^2/\Sigma w|F_o|^2]^{1/2}$; $w = 1/\sigma^2\{|F_o|\}$.

Mössbauer Spectroscopy Measurements. ^{57}Fe Mössbauer spectra (MS) were collected on crushed powder samples using a constant acceleration spectrometer equipped with a ^{57}Co(Rh) source kept at room temperature (RT). The spectrometer was calibrated with metallic Fe at RT, and the isomer shift (IS) values are expressed relative to this standard. A closed loop He cryostat (ARS) was used for the low temperature measurements.

Results and Discussion

Synthesis and Structure. $CaFe_4As_3$ can be rationalized as $(Ca^{2+})[(Fe^{2+})_3(Fe^{1+})(As^{3-})_3]$. We have attempted extensive experiments to modify complex anisotropic magnetic $CaFe_4As_3$ structure[18] by substituting Ca, Fe, and As atoms separately. We found out that the $CaFe_4As_3$ is very stable and not very prone to doping or substitution. It should be mentioned as well that not all possible atoms, which can be used as substituents, were exhausted. The substituting atoms were chosen on the basis of group−subgroup relationships, atomic radii, physical properties, the melting points of the elements and their miscibility, etc. For example, Ca and Sr are alkaline-earth metals from the same group, with similar coordination in many intermetallic compounds, but with slightly different atomic radii. Na has similar atomic radii to Ca; however, it can be only in oxidation state +1. In addition, P and Sb are above and below As in the Periodic Table. In most known intermetallic compounds, these three elements exhibit very similar coordination and bonding. However, the atomic radii of P and Sb are very different from that of As; thus, variations in the local coordination environments are possible, which subsequently may lead to new polymorphs of the $CaFe_4As_3$ structure type. In the attempts to substitute atoms at the Fe sites, consideration was taken also into identifying miscible transition metals with lower melting points in their phase diagrams. For example, the highest melting points in the Cr−Fe, Co−Fe, Zn−Fe, and Ni−Fe phase diagrams are below 1000 °C.

Figure 1. Projection view along the *b* axis of the structure of $CaCr_{0.84}$-$Fe_{3.16}As_3$.

In summary, attempts to substitute at the Ca site with Li, Na, K, Mg, Sr, La, Eu, and Yb led to the formation of $CaFe_4As_3$ and other known ternary or binary byproducts. In addition, none of the cations used in lieu of Ca produced an isostructural analog of $CaFe_4As_3$. These experiments indicate that the $CaFe_4As_3$ 3D-network is tailored only for Ca. Substitution at the As site was attempted with P and Sb, while at the Fe site, it was attempted with Zn, Co, In, Nb, and Ni. The outcome of these experiments was also negative as confirmed by energy-dispersive spectrometry (EDS) analysis. The specific size and electronic requirements to maintain the $CaFe_4As_3$ structure allowed only Cr substitution exclusively at the Fe(4) site, i.e., only the characterized Fe^{1+} ions in the $CaFe_4As_3$ structure were substituted by Cr^{1+}, as confirmed by neutron diffraction and Mössbauer analysis (see below). Thus, the $CaCr_{0.84}Fe_{3.16}As_3$ is the highest Cr content derivative composition available with the $CaFe_4As_3$ structure type, and several attempts to synthesize compounds with higher Cr content were not successful. Reactions designed to produce derivatives of the parent compound with Cr content larger than 1 yielded $CaCr_{0.84}Fe_{3.16}As_3$ and CrFeAs, as evident from EDS and PXRD. This is in sharp contrast with $BaCr_xFe_{2-x}As_2$ $(0 < x < 1)$[24] where Cr is incorporated extensively by a nonselective substitution.

$CaCr_{0.84}Fe_{3.16}As_3$ crystallizes in the orthorhombic space group *Pnma* with a 3-D framework, where Fe, Cr, and As form a covalent channel-like network with Ca^{2+} cations residing in the channels that run along the *b* axis of the orthorhombic cell; see Figure 1. The covalent network is made of Fe/As ribbons excised out of the Fe_2As_2 layers of $CaFe_2As_2$ and arranged in a rectangular cross pattern. The Fe_2As_2 layer is a common building unit of the structures of binary FeAs as well as the recently discovered superconducting layered materials. In the covalent network, three crystallographically distinct As sites, three Fe sites, and one site shared between Cr and Fe in the

(24) Sefat, A. S.; Singh, D. J.; VanBebber, L. H.; Mozharivskyj, Y.; McGuire, M. A.; Jin, R.; Sales, B. C.; Keppens, V.; Mandrus, D. *Phys. Rev. B* **2009**, *79*, 224524.

0.84−0.16 ratio were found. There are no bonding As−As interactions in the structure. The parallel PbO type Fe_2As_2 ribbons are connected through Fe(4) along the b axis to form the 3D-network.

The neutron time-of-flight Laue single crystal diffraction data were collected at 300 and 10 K, and there was no significant structural change observed between these two distinctive temperatures; see Table 1. These refinements were able to distinguish the location of the Cr atoms. In general, all structure parameters at 10 K were slightly smaller and proportional to their equivalents at ambient temperature. From this data, no indication for structural changes or structural transitions was found. For the structure refined with the 300 K data, the Fe−As distances fall into two different groups, depending upon the coordination of the Fe atoms. The short Fe−As distances, 2.394(2)−2.4938(15) Å, are found around Fe(1), Fe(2), and Fe(3) which are tetrahedrally coordinated by As(1), As(2), and As(3) (Table S4, Supporting Information). These distances are slightly longer than those found in $CaFe_4As_3$. The As−Fe−As angles between 93.63(5)° and 116.39(4)° for Fe(1), Fe(2), and Fe(3) deviate from the ideal tetrahedral angle (Table S4, Supporting Information). The second group of Fe−As distances around Fe(4)/Cr(4) is in the range of 2.461(3)−2.617(2) Å which is longer that those of the other Fe atoms because of the higher coordination number of Fe(4)/Cr(4) in a 5-coordinated square pyramidal geometry. The As−(Fe/Cr)−As angle in this geometry varies between 85.18(2)° and 104.67(4)°. The Ca^{2+} ions are sitting at the center of a mono-capped trigonal prismatic coordination by two As(1), two As(2), and two As(3) and additional capped As(3) atoms.

Charge Transport and Magnetism. Electrical resistivity measurements were performed in the range of 5−300 K on a single crystal of $CaCr_{0.84}Fe_{3.16}As_3$ parallel, ρ_b, and perpendicular (*ac* plane), ρ_{ac}, to the b axis in the crystal structure; see Figure 2. It should be noted that small amounts of residual tin were found on the crystal surface. Resistivity measurements on the same crystal were done after soaking it in 40% HCl for 12 h. The resistivity is higher compared to the first measurement, but the trend of both resistivity curves is identical (Figure S5, Supporting Information). The resistivity measurements from the first measurement are discussed here in order to keep consistency with the previous reports. The compound showed typical metallic behavior, i.e., resistivity falls as temperature decreases. The ρ_{ac} value ranges from 0.5 to 0.7 mΩ·cm, while the ρ_b value ranges from 0.02 to 0.12 mΩ·cm. The temperature dependent electrical resistivity (ρ_{ac}; see Figure 2a) has a distinct inflection point at 103 K, followed by a broad maximum at lower temperatures. Below 70 K, the decrease in resistivity is steeper. The ρ_b values showed no structure at 103 K (see Figure 2b) and monotonically decreased with decreasing temperature, becoming gradually steeper at lower T.

For comparison, the resistivity data for $CaFe_4As_3$ are also shown in Figure 2. The strong anisotropy in the electrical resistivity is preserved with the Cr for Fe substitution (on average, ρ_{ac} is six times higher than ρ_b). The major difference is observed in ρ_{ac}. The small peak at 23 K in ρ_{ac} data of $CaFe_4As_3$ is smaller, but noticeable, while it is missing in both
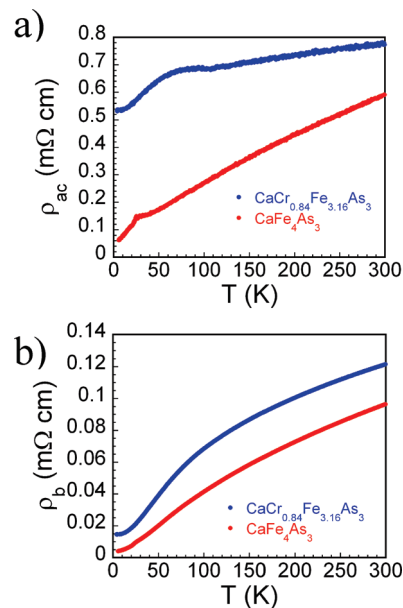
Figure 2. Electrical resistivity for a single crystal $CaCr_{0.84}Fe_{3.16}As_3$ measured (a) perpendicular (ρ_{ac}) and (b) parallel (ρ_b) to the b axis from 5 to 300 K. $CaCr_{0.84}Fe_{3.16}As_3$ (red) is compared with the parent compound $CaFe_4As_3$ (blue).
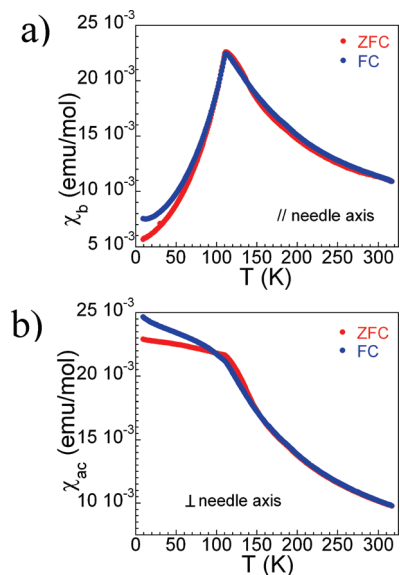
Figure 3. Anisotropic molar magnetic susceptibility measured (a) parallel (χ_b) and (b) perpendicular (χ_{ac}) to the needle direction of a single crystal $CaCr_{0.84}Fe_{3.16}As_3$ at 2000 Oe.

ρ_{ac} and ρ_b for $CaCr_{0.84}Fe_{3.16}As_3$. The higher electrical resistivity of $CaCr_{0.84}Fe_{3.16}As_3$ is probably associated with changes in the carrier scattering as a result of Cr incorporation and a possible decrease of the carrier concentration. This result is very different from what was observed in $BaCr_xFe_{2−x}As_2$ $(0 < x < 1)$[24] where the temperature dependent electrical resistivity manifests a sharp increase below 130 K and the temperature of this anomaly is diminished with increasing x.

Figure 3 shows the temperature dependence of the magnetic susceptibility (χ) of $CaCr_{0.84}Fe_{3.16}As_3$ single crystals in two orientations of the magnetic field, parallel (χ_b) and perpendicular (χ_{ac}) to the needle direction. At high temperatures ($T > 103$ K), there is no difference

between χ_b and χ_{ac}, indicating isotropic susceptibility. Below that temperature, a significant anisotropy in susceptibility shows up, suggesting an anisotropic magnetic interaction at this temperature region. Below 103 K, χ_b decreases very sharply, while χ_{ac} remains almost constant with decreasing temperature, indicating a Neel transition. This observation strongly suggests that the magnetic moments align with the *ac* plane. In comparison, magnetization measurements of $CaFe_4As_3$ showed two magnetic susceptibility SDW maxima at 23 and 96 K. Thus, the magnetic transition at 23 K has been smoothed out as a result of the Cr incorporation in the structure, specifically at the Fe(4) site. The 96 K transition shifts toward higher temperature, 103 K. This indicates that the SDW in the structure is intact and associated with the other three Fe atoms, a conclusion which is consistent with the results of the neutron derived magnetic structure of the SDW in $CaFe_4As_3$.[20]

The most noticeable difference between $CaFe_4As_3$ and $CaCr_{0.84}Fe_{3.16}As_3$ lies in their χ_{ac} values. In the parent compound, there is a hysteresis in the ZFC and FC χ_{ac} measurements up to room temperature.[18] This type of irreversibility is common for doped Cr alloys, and it was explained by the existence of a local spin-density wave associated with nonmagnetic impurities in Cr by including electron−impurity interactions.[25] Tugushev has reviewed the theory on this problem and showed that at some local temperature, T_{loc} above T_N, a local SDW may appear at an impurity or other structural defect, while its nature depends upon whether the long-range order that appears at T_N is a commensurate or incommensurate SDW.[26] In both cases, the local SDW will carry a local moment that will enhance the succeptibility between T_{loc} and T_N. In this aspect, the Cr substitution for Fe seems to simplify the complex magnetic structure of $CaFe_4As_3$ by suppressing these type of interactions; hence, the irreversibility in the ZFC and FC disappears. This partial preservation of the magnetic structure is possible only because Cr is not randomly distributed throughout the compound but concentrated exclusively at the Fe(4) site. In comparison, when Cr incorporates randomly in FeAs layers of $BaCr_xFe_{2-x}As_2$[24,27] ($x = 0.027-0.75$), the Neel transition is suppressed, SDW is destroyed, and with increasing x, a ferromagnetic state is approached and finally reached at the chemically ordered phase ($x = 1$).

Surprisingly, in $CaCr_{0.84}Fe_{3.16}As_3$, not only the Neel transition is preserved from that of $CaFe_4As_3$ but also it shifts to higher temperature. The resistivity behavior around T_N as well as neutron experiments currently in progress show that the ordering in $CaCr_{0.84}Fe_{3.16}As_3$ is also associated with a SDW transition. For a simple AFM metal, one would expect a drop in the resistivity below T_N, associated with loss of spin-disorder scattering. However, the resistivity of $CaCr_{0.84}Fe_{3.16}As_3$ has a weak minimum at T_N 103 K, Figure 2a, followed by a broad maximum at lower tempera-
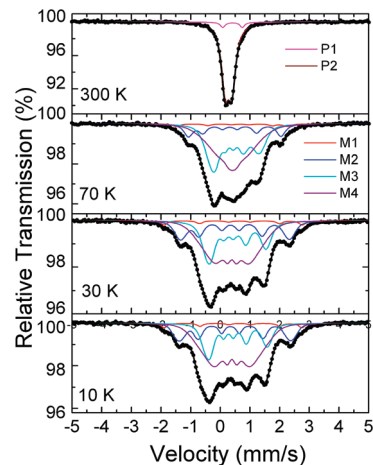
Figure 4. Mössbauer spectra of $CaCr_{0.84}Fe_{3.16}As_3$ collected at different temperatures. The points correspond to the experimental data and the continuous lines to the theoretical components used to fit the spectra. P1, P2, M1, M2, M3, and M4 denote the paramagnetic and the magnetic components.

tures, as observed in other typical SDW systems such as Cr and Cr−Ru.[28,29] In metallic Cr, this microscopic mechanism of the antiferromagnetic SDW was understood by the electron and hole interaction with opposite spins or the nesting of the Fermi surface below T_N. Then, substitution of Ru for Cr gives rise to an increase of electron density at Fermi energy and, accordingly, an increase of the nesting q space, so that T_N as well as the nesting wave vector rapidly increase. Further substitution suppresses the antiferromagnetic SDW probably due to the breakdown of this mechanism. The mechanism in the case of $CaCr_{0.84}Fe_{3.16}As_3$ is yet unclear. Finally, the magnetic moments calculated from the isotropic inverse susceptibility above the transition slightly differ from each other and are 5.87 and 5.44 B.M. or 1.46 and 1.36 B.M. per magnetic center for μ_b and μ_{ac}, respectively. These moments are lower than the expected spin only for 0.84 Cr^+, 0.16 Fe^+, and 3 Fe^{2+} and the reported magnetic moments for the parent compound.[18,19] This partial suppression of the effective magnetic moment is most likely due to anisotropy associated with crystal field effects. Interestingly, the reduced moment per Fe ion is also reminiscent of the Fe superconductors, for example, 0.4−0.8 μ_B/Fe for the ROFeAs compounds[30] and approximately 0.87 μ_B/Fe for $BaFe_2As_2$.[31]

Mössbauer Spectroscopy. Characteristic [57]Fe Mössbauer spectra (MS) of $CaCr_{0.84}Fe_{3.16}As_3$ collected at different temperatures are shown in Figures 4 and 5. The spectra acquire quadrupole paramagnetic splitting (QS) from 300 to 130 K. At this paramagnetic temperature region, the spectra can be fitted using two doublets (P1 and P2), in accordance with the corresponding spectra of $CaFe_4As_3$. The dominant doublet P2, which occupies about 95% of the

(25) Galkinyx, V.; Ortizy, W. A.; Fawcettz, E. *J. Phys.: Condens. Matter* **1997**, *9*, L557.
(26) Tugushev, V. V. *Itinerant Antiferromagnets in Electronic Phase Transitions*; Elsevier: Amsterdam, 1992.
(27) Bud'ko, S. L.; Nandi, S.; Ni, N.; Thaler, A.; Kreyssig, A.; Kracher, A.; Yan, J.-Q.; Goldman, A. I.; Canfield, P. C. *Phys. Rev. B* **2009**, *80*, 014522.

(28) Fawcett, E. *Rev. Mod. Phys.* **1988**, *20*, 209.
(29) Endoha, Y.; Chatani, K. *Phys. B* **2003**, *329*, 1077.
(30) de la Cruz, C.; Huang, Q.; Lynn, J. W.; Li, J.; Ratcliff, W., II; Zarestky, J. L.; Mook, H. A.; Chen, G. F.; Luo, J. L.; Wang, N. L.; Dai, P. *Nature* **2008**, *453*, 899.
(31) Huang, Q.; Qiu, Y.; Bao, W.; Green, M. A.; Lynn, J. W.; Gasparovic, Y. C.; Wu, T.; Wu, G.; Chen, X. H. *Phys. Rev. Lett.* **2008**, *101*, 257003.
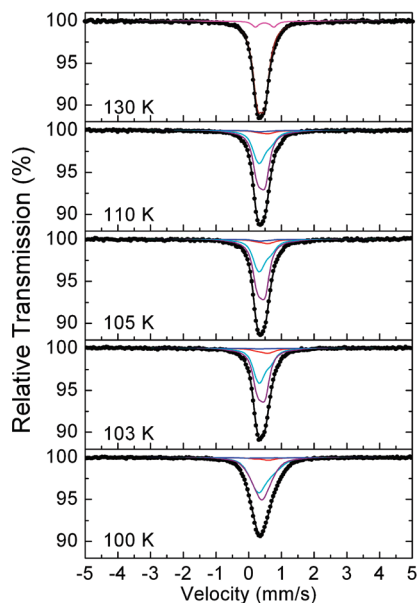
Figure 5. Mössbauer spectra of $CaCr_{0.84}Fe_{3.16}As_3$ recorded between 100 and 130 K.

absorption area in all paramagnetic spectra, has rather low IS and QS values, while the minor area component P1 possesses such higher values and accounts for the rest of the 5% of the absorption area. The IS and QS values are quite close to the corresponding values found for the two doublets of $CaFe_4As_3$. Thus, the Cr substituted phase contains both Fe^{2+} and Fe^+ ions, with the majority being Fe^{2+}.

Below 130 K, at 110 K, the spectra start to develop broadening of their absorption lines, which might indicate onset of magnetic order. However, between 110 and 103 K, the spectra attain almost the same broad line characteristics, and at 100 K, an even larger broadening appears; see Figure 5. This is more solid evidence of onset of magnetic order, but distinct contributions from six-line patterns do not appear before 90 K. The complete development of all magnetic contributions is clearer at the 30 K spectrum, Figure 4. We used a set of four magnetically split components to describe this spectrum adequately. Three of these components (M2, M3, and M4) have relatively low IS values, and their absorption areas sum up to 97%, while the remaining component M1 has larger IS and B_{hf} values compared with the former. The IS values in this temperature relate to the corresponding values of the paramagnetic temperature region by the expected increase attributed to the second-order Doppler shift (Figure S1, Supporting Information). The correspondence connects the minor sextet M1 to the minor doublet P1 and the set of the three major sextets (M2−M4) to the major doublet P2, respectively. Applying this analysis model to all magnetically split spectra between 10 and 100 K, we have attained a very good characteristic set (Figure S2, Supporting Information). The spectra between 103 and 110 K can be fitted with either two doublets, as in the paramagnetic temperature region, or with four sextets (see Figure 5), giving however quite low B_{hf} values to all components in the second case. The magnetically split components model has given fits with lower residual (χ^2) values than the paramagnetic one for these

spectra, suggesting the existence of magnetic order at these temperatures.

The magnetic splitting and the paramagnetic MS of Ca-$Cr_{0.84}Fe_{3.16}As_3$ indicate the presence of both Fe^{2+} and Fe^+ in its structure, as in the case of the parent compound $CaFe_4As_3$. However, the main characteristic which results from the comparison of the set of spectra for these two compounds is the large reduction of the absorption area of the minor component (doublet or sextet(s) in the paramagnetic or magnetic temperature regions, respectively). This component is attributed to the Fe^+ ions. This finding confirms that the substitution of Fe by Cr involves mainly the characterized Fe^+ ions (Fe(4) site) of the $CaFe_4As_3$ structure.

From the point of view of Mössbauer spectroscopy, it is seen that there are no major changes in the shape of the spectra and in the B_{hf} and quadrupole shift (2ε) values at 25 K (Figures S2 and S3, Supporting Information), with an exception of the diversification of the 2ε values for the M2 and M3 components below 50 K. This means that the structure transition found for $CaFe_4As_3$ at around 25 K has been suppressed by the substitution of some of the Fe^+ ions by Cr^+. On the other hand, the magnetic ordering temperature seems to have shifted to higher values than that of the parent $CaFe_4As_3$ (T_M = 90 K), by an interval of 10−40 K. Another characteristic of the substituted $CaCr_{0.84}Fe_{3.16}As_3$ is the presence of one instead of two distinct Fe^+ components in the magnetic temperature region. Following the discussion of the origin of the two Fe^+ components of the parent $CaFe_4As_3$, this involves a substitution of almost all iron ions of the Fe(4) site by Cr.

Conclusion

The new iron arsenide, $CaCr_{0.84}Fe_{3.16}As_3$ is isostructural to $CaFe_4As_3$. Cr is not randomly distributed in the structure but rather is concentrated exclusively at the Fe(4) site. Because of the preferential substitution of Fe^+ with Cr^+ at the Fe(4) site, the magnetic and resistivity properties resemble undoped $BaFe_2As_2$ phases rather than its Cr-doped analog where the distribution of Cr in the crystal structure is random. This type of targeted Cr-doping limits the interaction between the Fe spins to a short-range and surprisingly preserves the AFM and SDW transitions from the parent compound $CaFe_4As_3$. Apparently, SDW of the $CaFe_4As_3$ material is robust and could not be disrupted through Cr doping.

Supporting Information Available: X-ray crystallographic files, atomic positions (Table S1), anisotropic displacement parameters (Table S2), selected bond lengths and angles (Table S3), isomer shift values as resulting from the best fits of the Mössbauer spectra (Table S4), quadrupole splitting (QS) and quadrupole shift (2ε) values as resulting from the best fits of the Mössbauer spectra (Table S5), hyperfine magnetic field

values as resulting from the best fits of the Mössbauer spectra (Table S6), values of the spreading of the hyperfine magnetic field as resulting from the best fits of the Mössbauer spectra (Table S7), relative absorption area values as resulting from the best fits of the Mössbauer spectra (Table S7), temperature variation of the IS values (Figure S1) Mössbauer spectra (Figure S2), temperature variation of the quadrupole splitting (Figure S3) and temperature variation of the hyperfine magnetic fields (PDF, CIF). This material is available free of charge via the Internet at http://pubs.acs.org.